NMR structure of the *Aquifex aeolicus* tmRNA pseudoknot PK1: new insights into the recoding event of the ribosomal trans-translation

Sylvie Nonin-Lecomte*, Brice Felden[1] and Frédéric Dardel

Université Descartes Paris V - Faculté de Pharmacie, Laboratoire de Cristallographie et RMN Biologiques, CNRS UMR 8015, 4, av. de l'Observatoire—75006 Paris, France and [1]Université de Rennes I, UPRES JE2311, Inserm ESPRI ERI6, Biochimie Pharmaceutique, 2 avenue du Prof. Léon Bernard – 35043 Rennes, France

ABSTRACT

The transfer-messenger RNA (tmRNA) pseudoknot PK1 is essential for bacterial trans-translation, a ribosomal rescue mechanism. We report the solution structure of PK1 from *Aquifex aeolicus*, which despite an unprecedented small number of nucleotides and thus an unprecented compact size, displays a very high thermal stability. Several unusual structural features account for these properties and indicate that PK1 belongs to the class of ribosomal frameshift pseudoknots. This suggests a similarity between the mechanism of programmed ribosomal frameshifting and trans-translation.

INTRODUCTION

To deal with translation failures caused by defective messages, bacteria have evolved a ribosome rescuing system called trans-translation [for reviews see (1,2)]. During this process, a transfer-messenger RNA molecule (tmRNA) complexed to the proteins SmpB and EF-Tu-GTP binds to the ribosome and acts both as a tRNA and as an mRNA, to release incompletely translated messages. The incomplete polypeptides are end-labeled by a tag encoded in an internal open reading frame (iORF) of the tmRNA and are targeted for degradation.

The secondary structures of bacterial tmRNAs have been deduced from comparative sequence analyses (3–5), showing that they contain a tRNA-like domain (TLD) joining the 3′ and 5′ ends of the molecule, an iORF encoding the degradation peptide tag, and four pseudoknots (PK1-PK4). The crystal structure of the *Escherichia coli* TLD–SmpB complex (6) is the only detailed structure obtained to date for one of the structural domains of the tmRNA. Of the four pseudoknots, only PK1, which flanks the resume codon, is essential for trans-translation (7) and is conserved in all the known tmRNA gene sequences. In the pre-accommodation state into the P-site of the ribosome, PK1 points towards the channel entry of the 30S subunit (8). A consensus secondary structure has been proposed for PK1, based on phylogenetic studies, structural probing and NMR analyses (4,9). PK1 belongs to the H-type pseudoknot category (10) with a first GC-rich stem and a partly conserved L2 loop carrying a UAAAA-like sequence. With 21 nt, the PK1 from the thermophilic bacterium *Aquifex aeolicus* is predicted to be the smallest of all tmRNAs (11) (Figure 1a), being actually shorter than the absolute minimal predicted size for pseudoknots (12) (≥22 nt). This paper describes the detailed NMR structure of the *A.aeolicus* PK1. It exhibits a number of critical features, which are common to frameshift-inducing pseudoknots from eukaryotic viruses. For the first time, this provides evidence that these two types of ribosome reprogramming mechanisms could share common features.

MATERIALS AND METHODS

Samples preparation

Unlabeled 22mer RNA oligonucleotides were purchased from MWG Biotech. The uniformly ^{13}C, ^{15}N labeled RNA was enzymatically synthesized by Silantes. All samples were dialyzed several times against NaCl and EDTA and finally extensively against deionized water. The pH was adjusted between 6 and 6.5 before freeze-drying.

NMR methods

The NMR samples were prepared by re-suspension in either 95% H_2O / 5% D_2O or D_2O buffers. A total of 0.5 mM EDTA was added to prevent sample degradation and pH was re-adjusted to 6.3 before introduction in a Shigemi NMR tube. Strand concentrations of the different NMR samples checked by ultraviolet (UV) absorbance at 260 nm ran between 0.7 and 1 mM. The NaCl concentration is 50 mM.

---

*To whom correspondence should be addressed. Tel: +33 1 53 73 15 74; Fax: +33 1 53 73 99 25; Email: sylvie.nonin@univ-paris5.fr

NMR experiments were conducted on a 600 MHz Bruker Avance spectrometer equipped with Z-gradients and a triple resonance TXI probe. All spectra were processed and analyzed using Felix 2000.1 (Molecular Simulations Inc.).

The resonances were assigned using the usual set of 2D and 3D homo- and hetero-nuclear NMR methods in D_2O and in 95% H_2O / 5% D_2O: 2D NOESY with 20, 40, 60, 90, 150 and 300 ms mixing times, 2D TOCSY, 2D $^{13}C^1H$-HSQC, 2D constant-time ^1H-^{13}C-HSQC, 2D ^1H-^{13}C- long-range HSQC, 2D ^1H-^{13}C-HMBC, 2D ^1H-^{15}N-HMBC, 2D ^1H-^{15}N-TROSY, 3D NOESY-HMBC and 3D NOESY-HSQC. Solvent suppression in H_2O buffer was achieved using either Jump-and-Return pulse sequence, or water flip-back Watergate or gradient sculpting.

Base pairings were established from $^2J_{NN}$ HNN-COSY (13). The absence of unusual base pairs involving purine N7 or N9 were probed by $^2J_{NH}$ HNN-COSY in D_2O (14). Hydroxyl protons were identified as exchangeable protons which still appear at single proton frequency on undecoupled JR-NOESY spectra. They also yield no signal in the J_{NN} HNN-COSY experiment. The H2 and H8 protons of the adenines were connected by HCCH-TOCSY with DIPSI duration of 72 ms. Intranucleotide H1′-to-base proton correlations were obtained in a 2D HCN experiment (15). Sugar spin systems assignments were performed using 3D HCCH-E.COSY and ≪ directed ≫ HCC-TOCSY-CCH-E.COSY (16) experiments. Inter-proton distances derived from NOE cross-peak volumes measured at short mixing times were sorted into four categories, very strong [1.8–2.8 Å], strong [2.5–3.5 Å], medium [3.2–4.5 Å], weak [3.5–5.5 Å] and very weak [3.5–7 Å], based on comparisons with cytosine H5-H6 cross-peaks. For intra sugar NOEs, the very strong range was shifted to [2.0–3.2 Å]. Torsion angle values were derived from the analysis of the HCCH–E. COSY and HCC-TOCSY-CCH E-COSY optimized for analysis of $^3J_{H1′H2′}$ and $^3J_{H3′H4′}$ coupling constants, and NOESY spectra. The intra-residue H8/H6-H1′ and H8/H6-H3′ cross-peaks volumes indicate that all bases are in the anti conformation (Chi angles were thus restrained to 202 ± 30). Torsion angles values ν_0 to ν_4 were restrained to the C2′-endo conformation within 60° for residues with $^3J_{H1′-H2′}$ couplings >3 Hz and $^3J_{H3′-H4′}$ couplings <7 Hz, (i.e. U5, U9, C13 and U14), and to the C3′-endo conformation for residues with $^3J_{H1′-H2′}$ couplings <3 Hz and $^3J_{H3′-H4′}$ coupling >7 Hz. G19 pucker was not constrained due to uncertainties in the coupling measurements flowing from spectral overlap.

The PK1 stems 1 and 2 are well defined. Their respective orientations are fixed on one hand at the junction by many NOE constraints within the 'A-box', and on the other by loop 2 which interacts with the minor groove of stem 1 and which last residue A18 is clamped inside the 'A-box'. Thus they can be considered as being part of a single structural domain. Because in this particular case, the gain in RMSD is expected to be small, we did not run RDC measurements.

Melting temperature

The melting temperature experiments were recorded on a Beckman DU 640B spectrophotometer, by following the UV absorbance at 260 and 280 nm. The temperature was controlled by a Beckman 'High Performance Temperature Controller'. The temperature was increased from 15° to 95°C at a rate of 0.2°C/min.

Structure computation

Structure calculations were performed for the 22mer PK1, using the CNS dynamical annealing protocol for nucleic acids, using NOE and dihedral angle restrains. Starting from a randomized extended strand, 100 structures were generated after the four following stages: (i) 30 ps of restrained torsion angle dynamics (TAMD) at 20 000 K during the high-temperature annealing stage; (ii) 40 ps of TAMD during a first cooling stage in which the van der Waals scale energy scale factor is increased from 0.1 to 1; (iii) 35 ps of restrained molecular dynamics during a second slow-cool annealing stage in which the van der Waals scale energy scale factor is increased from 1 to 4; (iv) ten cycles of energy minimization of 300 steps each. All structures were then entered into an energy minimization protocol, which starts with 10 ps TAMD at 300 K, followed by cooling over 9 ps and 10 Powell cycles of 800 steps each. Out of 100 computed structures; the fifteen structures of lower overall energy were selected, with the convergence criteria listed in Table 1. The MOLMOL program (17) was used for structure analysis and figure preparation.

RESULTS AND DISCUSSION

Stability and solution structure of PK1

Contrasting with its minimal size, this pseudoknot exhibits an exceptional stability. Its melting temperature is 56°C in

Table 1. NMR and refinement statistics for the *A.aeolicus* PK1

NMR distance and dihedral constraints	
Distance restraints	
Total NOE	250
Intra-residue	100
Inter-residue	108
Sequential ($\lvert i-j \rvert = 1$)	71
Non-sequential ($\lvert i-j \rvert > 1$)	37
Hydrogen bonds	42
Total dihedral angle restraints	123
($\chi, \nu_0, \nu_1, \nu_2, \nu_3, \nu_4$)	
Structure statistics[a]	
Violations (mean ± s.d.) for the average structure	
Distance constraints (Å)	0.04 ± 0.01
Dihedral angle constraints (°)	0.14 ± 0.02
Maximum dihedral angle violation (°)	5
Maximum distance constraint violation (Å)	0.25
Deviations from idealized geometry	
Bond lengths (Å)	0.0021 ± 0.00006
Bond angles (°)	0.6769 ± 0.0047
Impropers (°)	0.3780 ± 0.0096
Number of Van der Waals violations (cut off 1.6 Å)	0
r.m.s.d. (Å)	
Average r.m.s.d (for all heavy atoms, fit to mean)	0.94
Helix 1	0.65
Helix 2	0.67
'A-box' (G4, U5, C8, C10, A18, G19)	0.63
U9	0.73
Loop2 (U14–C17)	1.63

[a]Calculated for the 15 refined lowest-energy structures.

50 mM NaCl and rises to 73°C with 1 mM MgCl₂ added. Comparatively, the longer 26mer PLRV (Potato leaf roll virus) pseudoknot has a T_m of only 50°C in more stabilizing conditions [150 mM NaCl, 2 mM MgCl₂, (11)]. Structural features beyond secondary structure are thus likely to contribute to its stability. We solved the solution structure of a 22mer oligoribonucleotide corresponding to the PK1 of *A.aeolicus* tmRNA (Figure 1a). Essentially complete ¹H resonances were assigned using standard heteronuclear NMR strategies [for a review see (18)]. The average structure and the set of converged conformers (for statistics see Table 1) are shown in Figure 1b and c. The structure reveals a number of interesting features. It is very compact with an extensive level of base stacking, neatly organized along three parallel axes (Figure 2a and b). Only two of the 22 nt, U9 and C17, are excluded. Detection of ²J_{NN} couplings across hydrogen bonds reveals that the structure comprises only seven Watson–Crick GC pairs (Figure 3a). They are arranged in two stems adopting

the standard A helix geometry, in keeping with the observed sequential NOEs. A JR-NOESY spectrum recorded with a 20 ms mixing time shows that the terminal pair G1·C13 is formed (see Supplementary Figure 1). The predicted A18–U9 pair (Figure 1a) is not formed. The ejection of U9 allows formation of a long trans-helical axis spanning the whole pseudoknot structure. At the junction, C8 and C10 stack very well on each other and the helical axes of the two stems are almost collinear.

Non-canonical interactions

Most residues that are not part of the stems are engaged in non-canonical interactions, which translate into many unusual patterns on the NMR spectra. For example several adenine and guanine amino protons (G2, G3, A18) are resolved (Figure 3b), strongly indicative of extensive hydrogen bonding. Two hydroxyl sugar protons (U5 and C10) are protected
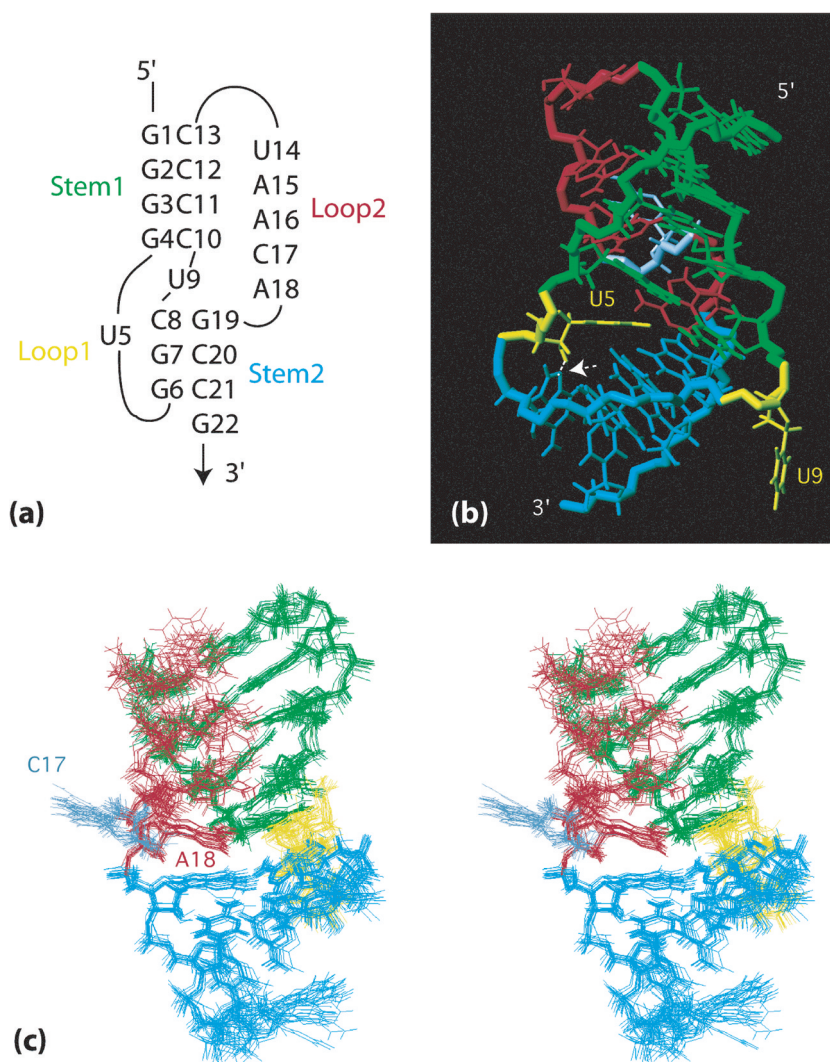

Figure 1. *A.aoelicus* PK1 sequence and structure: (**a**) Nucleotide sequence of PK1. To improve *in vitro* transcription, nucleotides C1 and G13 were permuted. Wild-type and permuted sequences yield similar NMR spectra. G22 was included to reduce minor forms. (**b**) View of the average structure of PK1. The U-turn between U5 and G6 is maintained by a ribose-zipper H-bond between U5 OH2′ and G6 N7 (arrow head). G22, phosphate oxygens and H5′/H5″ are not displayed. Color coding: green: stem 1, cyan: stem 2, red: loop 2 except for C17 (grey), yellow: U5 and U9. (**c**) Superposition of the 15 converged NMR structures, using same color coding as in (b), after counterclock rotation by 75° around the vertical axis.
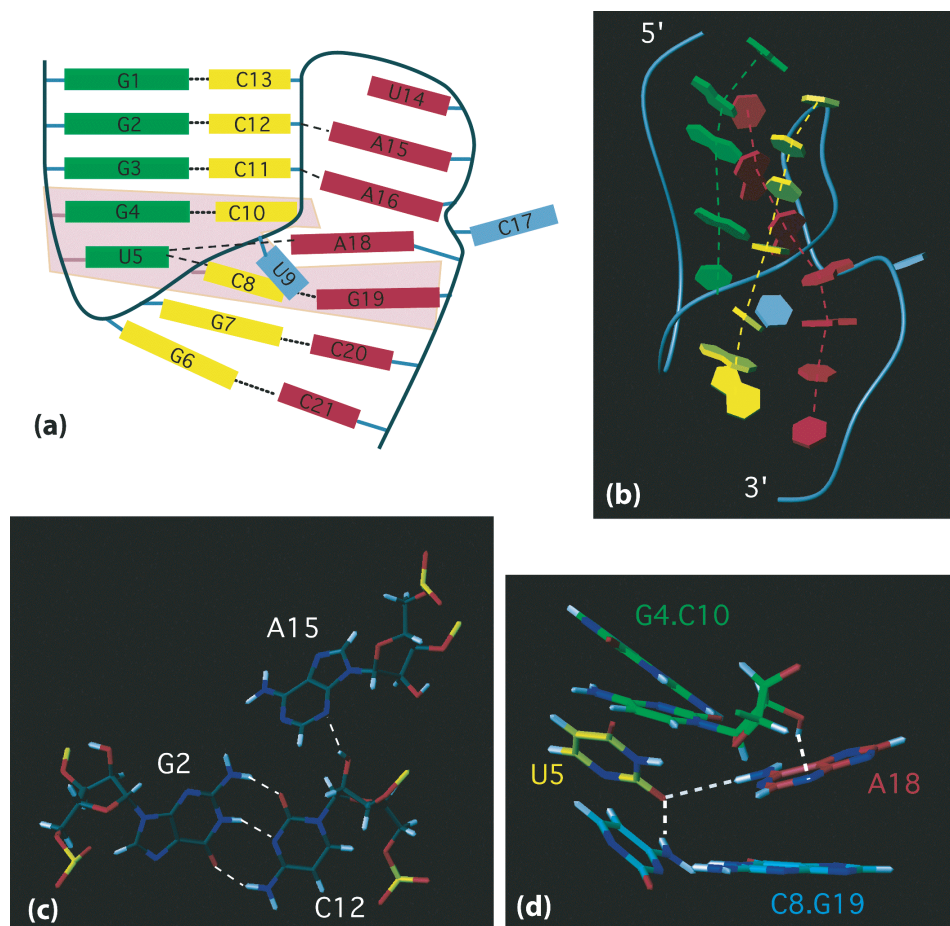
Figure 2. Structural features of the PK1: (**a**) Schematics of the structure showing the three axes of stacking. Doted lines: Watson–Crick base pairings. Dashed lines: non-canonical base interactions. The box around A18 is displayed on a pink background. (**b**) The three axes of stacking in the average structure are symbolized by colored dotted lines using same coding as in (a). (**c**) Interactions between A15 and G2·C12. (**d**) The three non-canonical H-bonds within the 'A box'. Color coding as in Figure 1.

from rapid exchange with water (Figure 3b). They yield narrow linewidth resonances at respectively 10.8 and 9.75 p.p.m., which are downfield shifted by more than 3 p.p.m. compared to the chemical shift of the hydroxyl resonances in poly(rI)·poly(rC) (6.33 p.p.m.) and poly(rA)·poly(rU) (6.61 p.p.m.) (19). These observations are reminiscent of the slowly exchangeable G34 OH2′ proton observed by NMR in the complex between the ATP and the AMP RNA aptamer (20). In this case, the G34 OH2′ was H-bonded an adenine N7. Similarly, our data support strong hydrogen bonding to a nitrogen acceptor.

Loop L2 is well organized; its nucleotides are stacked on top of each other and face the minor groove of helix 1. The cross-peaks between A15 H2 and G2 H21/H22 show that A15 forms a base triple with G2–C12 (Figure 3b). The huge chemical shift separation between the two G2 amino proton resonances strongly supports hydrogen bonding. As the average distance between G2 H21/22 and A15 N1 is about 3 Å, the interaction probably occurs via a water molecule (Figure 2c). A similar interaction between A16 and G3·C11 is expected from the cross-peaks observed between A16 H2 and G3 H21/H22 (Figure 3b).

A single nucleotide, U5, spans the major groove of stem 2. The H-bond between U5 OH2′ and G6 N7 is associated with

the observation of two cross-peaks on the NOESY spectrum (U5 OH2′/G6 H8 and U5 OH2′/G6 H2′, Figure 3b). This interaction stabilizes a backbone U-turn (Figure 1b). U5 also forms a distorted triple with via the major groove side of the C8–G19 pair (Figure 2d). U5 N3H yields a weak cross-peak with G4 N1H, consistent with the fact that U5 is turn inwards and stacked under G4 (Figure 1b, and U5 H6/G4 H6 and U5 H6/G4 H1′ cross-peaks on Supplementary Figure 2). The average distance measured between U5 N3H and A18 N1 is 3 Å, which is too large for strong base pairing. However, the imino proton exchange rate of U5 N3H with water is reminiscent of the exchange properties of the imino protons from terminal base pairs (21). It can be explained by intrinsic catalysis (22) by the A18 N1 nitrogen ($pK_a = 3.8$ at 25°C) coupled with a high dissociation constant. U5 N3H is thus most probably engaged in a weak hydrogen bond association with A18 N1, maybe relayed by a water molecule. Similar fast exchanging and non-terminal imino protons engaged in weak H-bond associations have been described in the litterature in RNA (23) and DNA (24) structures.

Adenine A18 appears to play a critical role. Its aromatic protons are NOE-connected to G19 and C10 (Supplementary Figure 2). A18 is the most buried residue of the structure, with only about 18% of its surface accessible to the solvent. By
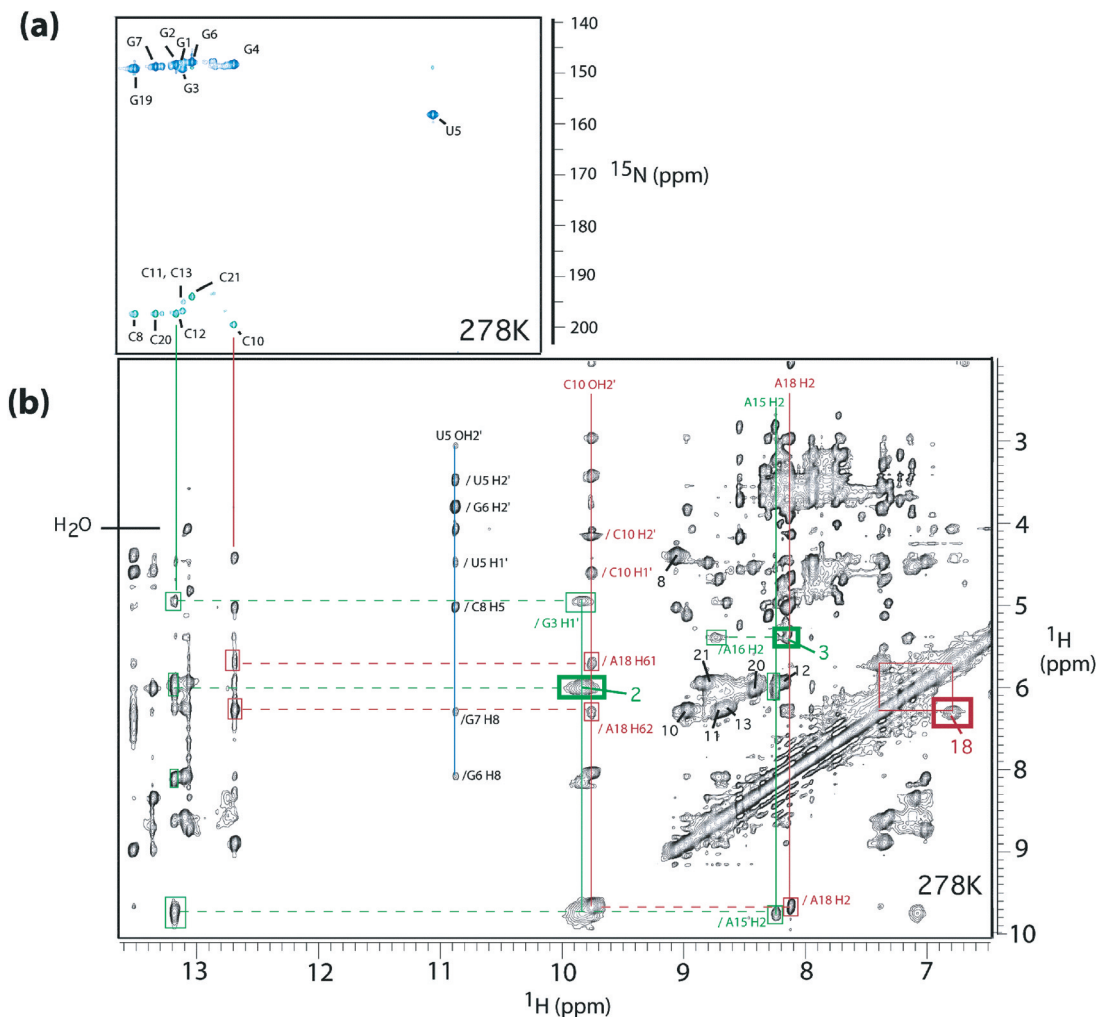
Figure 3. Selected NMR spectra showing the exchangeable proton resonances (imino, amino and hydroxyl) of the PK1 structure: (**a**) Imino proton region of the HNN-COSY spectrum recorded at 278 K with the coupling delay set to 15 ms. Direct $^1J_{NH}$ couplings yield blue cross-peaks. $^{2h}J_{NN}$ couplings through GN1H-CN3 hydrogen bonds yield opposite-sign cross-peaks displayed in green. (**b**) Example of connection pathways observed within the exchangeable proton region of a 150 ms mixing time JR-NOESY recorded at 278 K. Some of the specific interactions determining the local geometry are boxed (red lines and boxes for the A-box, green lines and boxes for the A15/G2·C12 triple, blue line for U5 OH2′ interactions stabilizing the U-turn). Intra-residue amino/amino cross-peaks are labeled by the residue number in black for cytosines, in green for G2 and in red for A18.

comparison, stem residues have 30 to 40% accessibility. It lies within what we call an 'A-box', the side panels of which are made by C8–G19 and G4–C10 pairs, with U5 at the bottom (Figure 2d). A18 is clamped deep inside via a hydrogen bond between the U5 2-oxo-group and one of its amino protons, and maintained by a ribose-zipper-like H-bond between C10 OH2′ and A18 N3 (Figure 2d). This interaction is experimentally supported by the two cross-peaks observed between C10 OH2′ and A18 H61/H62 amino protons (Figure 3b). Such a 'ribose-zipper' has already been observed in RNA structures, for instance within the HDV ribozyme (25). The unusual geometry of the 'A-box' induces a large helical twist at the junction of the two stems (∼115°).

Comparison with other tmRNA PK1

The adenines in the UAACA segment contribute most of the stabilizing tertiary interactions, participating to the A-box at the stem junction, to the extensive stacking and to base triple

formation. This sequence is fairly well conserved (26), suggesting that other bacterial tmRNA could share a similar PK1 structure. *E.coli* PK1 is expected to closely resemble that of our structure, with two GC-rich stems and an A-rich loop closing stem 1 from the minor groove. A single residue (equivalent of our U5) would also span stem 2. The comparison of the two sequences suggests that guanines G61 and/or G62 (equivalent to U9) should be excluded from the structure. Interestingly, mutations of these residues, as well as those within loop 2, and at the junction within the equivalent of the 'A-box', resulted in an impaired *E.coli* tmRNA tagging activity *in vitro* (7,27).

Comparison with other pseudoknots

The compact PK1 structure is quite different from that of long pseudoknots, such as the TYMV pseudoknot (28), but shares a number of striking similarities with the short viral pseudo-knots involved in programmed ribosomal frameshifting

(Figure 4a and b) (11) like the Beet western yellow virus (BWYV) and PLRV frameshift-inducing pseudoknots, which are also compact pseudoknots (28 and 26 nt, respectively). The *A.aeolicus* PK1, together with the PLRV and the BWYV pseudoknots, are the three smallest pseudoknots whose structures have been solved. We could not find in the literature any pseudoknot of smaller length. These three pseudoknots share a small number of base pairs involved in the two stems (seven for the PK1 and the PLRV and eight for BYWV) compared to other pseudoknots like SRV1 e.g. [12 bp, 34 nt (29)], MMTV [11 bp, 33 nt (30)] and TYMV pks [13 bp, 40 nt (28)]. Other common features include extensive stacking, stabilization of the stem junction by a triple, exclusion of a uridine (U9) at the junction and insertion of the L2 loop in the minor groove of stem 1. However, of the three short pseudoknots, PK1 has the shortest connecting loops: 1 (loop 1) and 5 (loop 2) nucleotides versus 2 and 9, and 2 and 7 respectively for the PLRV and the BWYV pseudoknots. PK1 specific features include the A-box and the minimal length in which all these non-canonical interactions are squeezed. Based on comparisons between BWYV and PLRV, a minimal size of 22 nt was inferred for frameshift pseudoknots (11). As a result of its densely packed core, the *A.aeolicus* PK1 is actually 1 nt shorter. Interestingly, for the PLRV pseudoknot, loop 2 and the excluded uridine (Figure 4b) have been shown to play a key role in the frameshifting efficiency, in addition to the pseudoknot resistance to ribosome unwinding. It has thus been suggested that the corresponding residues could establish specific interactions with the ribosome, thereby promoting the slippage (11).

CONCLUSION

The main intriguing questions regarding trans-translation and tmRNA function are (i) What is the sequence of events leading to the switch of template from the defective mRNA to the tmRNA by the ribosome? and (ii) How does the ribosome line up correctly with the resume codon in the iORF? PK1 is the only essential pseudoknot for trans-translation and hence is expected to participate to either or both of these processes. Our structural data suggest that trans-translation and programmed frameshifting could proceed via similar molecular mechanisms: PK1 and frameshift pseudoknots share common structural features like a GC-rich stem interacting with an A-rich loop, and a looped-out residue at the junction. As discussed above, these features have been shown in both cases to play an important functional role in the respective ribosome recoding events. Furthermore PK1 is located at the 30S mRNA channel entry in the pre-accommodation step (8), i.e. in a location similar to that of the frameshift pseudoknots while the ribosome is decoding the 'slippery' sequence. These striking similarities suggest that the pseudoknot interactions with the ribosome could be similar, and in particular could involve the essential looped-out residue at the stem junction.

During trans-translation process, the TLD has to move to the P-site after the first peptidyl transfer occurs, and then the iORF has to penetrate into the A site in the decoding centre. This is a topologically complex process, as the tmRNA is a circular molecule, with a large internal loop containing the iORF. Recent studies suggest that the tmRNA can pass through the ribosome without destruction of its pseudoknots, which should be located on the solvent side of the 30S subunit during
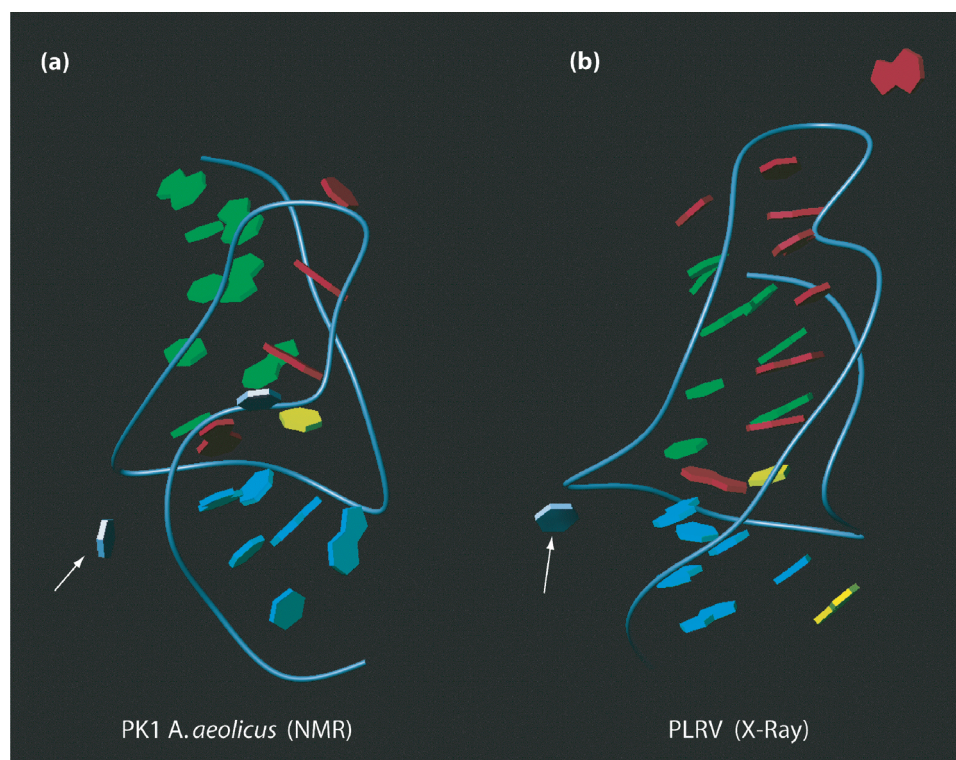

Figure 4. Comparison between the PK1 and the PLRV pseudoknots: Schematics using same color coding as in Figure 1 with the exception of 'rejected' residues which are displayed in grey. (**a**) NMR structure *A.aeolicus* PK1. (**b**) X-ray structure of the PLRV (11). An arrow points the important looped-out residues.

the whole trans-translation process (31). This was recently confirmed for PK3 (32). However, in the unnatural context of altered tmRNAs lacking internal stop codons, PK2, PK3 and PK3 are unfolded and transcribed (33). The crystal structure of the 70S *Thermus thermophilus* ribosome complexed with an mRNA shows that the distance from the first base of the P-site codon to the opening at which the mRNA enters the ribosome is about 13–15 nt long (34). This means that in shifty mRNAs, the first nucleotides of stem 1 and of loop 2 of the pseudoknots are engaged in the channel entry while the ribosome is on the slippery sequences, which are about 6 to 7 nt upstream. The PK1 could likewise anchor the tmRNA into the ribosome via similar interactions with the channel entry. Conversely to programmed frameshifting, PK1 is not downstream but upstream the sequence to be translated. In this configuration, PK1, which is believed to exhibit resistance to unwinding, could serve as a pawl or a peg around which the rest of the molecule would rotate during translation of the iORF.

SUPPLEMENTARY DATA

Supplementary Data are available at NAR Online.

REFERENCES

1. Saguy,M., Gillet,R., Metzinger,L. and Felden,B. (2005) tmRNA and associated ligands: a puzzling relationship. *Biochimie*, **87**, 897–903.
2. Haebel,P.W., Gutmann,S. and Ban,N. (2004) Dial tm for rescue: tmRNA engages ribosomes stalled on defective mRNAs. *Curr. Opin. Struct. Biol.*, **14**, 58–65.
3. Williams,K.P. and Bartel,D.P. (1996) Phylogenetic analysis of tmRNA secondary structure. *RNA*, **2**, 1306–1310.
4. Felden,B., Himeno,H., Muto,A., McCutcheon,J.P., Atkins,J.F. and Gesteland,R.F. (1997) Probing the structure of the *Escherichia coli* 10Sa RNA (tmRNA). *RNA*, **3**, 89–103.
5. Gueneau de Novoa,P. and Williams,K.P. (2004) The tmRNA website: reductive evolution of tmRNA in plastids and other endosymbionts. *Nucleic Acids Res.*, **32**, D104–D108.
6. Gutmann,S., Haebel,P.W., Metzinger,L., Sutter,M., Felden,B. and Ban,N. (2003) Crystal structure of the transfer-RNA domain of transfer-messenger RNA in complex with SmpB. *Nature*, **424**, 699–703.
7. Nameki,N., Tadaki,T., Himeno,H. and Muto,A. (2000) Three of four pseudoknots in tmRNA are interchangeable and are substitutable with single-stranded RNAs. *FEBS Lett.*, **470**, 345–349.
8. Valle,M., Gillet,R., Kaur,S., Henne,A., Ramakrishnan,V. and Frank,J. (2003) Visualizing tmRNA entry into a stalled ribosome. *Science*, **300**, 127–130.
9. Metzinger,L., Hallier,M. and Felden,B. (2005) Independent binding sites of small protein B onto transfer-messenger RNA during trans-translation. *Nucleic Acids Res.*, **33**, 2384–2394.
10. Hilbers,C.W., Michiels,P.J. and Heus,H.A. (1998) New developments in structure determination of pseudoknots. *Biopolymers*, **48**, 137–153.
11. Pallan,P.S., Marshall,W.S., Harp,J., Jewett,F.C., IIIrd, Wawrzak,Z., Brown,B.A., IInd, Rich,A. and Egli,M. (2005) Crystal structure of a luteoviral RNA pseudoknot and model for a minimal ribosomal frameshifting motif. *Biochemistry*, **44**, 11315–11322.
12. Giedroc,D.P., Theimer,C.A. and Nixon,P.L. (2000) Structure, stability and function of RNA pseudoknots involved in stimulating ribosomal frameshifting. *J. Mol. Biol.*, **298**, 167–185.
13. Dingley,A.J. and Grzesiek,S. (1998) Direct observation of hydrogen bonds in nucleic acid base pairs by internucleotide $^2J_{NN}$ couplings. *J. Am. chem. Soc.*, **120**, 8293–8297.
14. Hennig,M. and Williamson,J.R. (2000) Detection of N-H...N hydrogen bonding in RNA via scalar couplings in the absence of observable imino proton resonances. *Nucleic Acids Res.*, **28**, 1585–1593.
15. Sklenar,V., Peterson,R.D., Rejante,M.R. and Feigon,J. (1993) Two- and three-dimensional HCN experiments for correlating base and sugar resonances in 15N, 13C-labeled RNA oligonucleotides. *J. Biomol. NMR*, **3**, 721–727.
16. Schwalbe,H., Marino,J.P., Glaser,S.J. and Griesinger,C. (1995) Measurement of H,H-coupling constants associated with ν1, ν2 and ν3 in uniformly ^{13}C-labeled RNA by HCC-TOCSY-CCH-E.COSY. *J. Am. Chem. Soc.*, **117**, 7251–7252.
17. Koradi,R., Billeter,M. and Wuthrich,K. (1996) MOLMOL: a program for display and analysis of macromolecular structures. *J. Mol. Graph*, **14**, 51–5529–32.
18. Furtig,B., Richter,C., Wohnert,J. and Schwalbe,H. (2003) NMR spectroscopy of RNA. *Chembiochem.*, **4**, 936–962.
19. Leroy,J.L., Broseta,D. and Gueron,M. (1985) Proton exchange and base-pair kinetics of poly(rA).poly(rU) and poly(rI).poly(rC). *J. Mol. Biol.*, **184**, 165–178.
20. Jiang,F., Kumar,R.A., Jones,R.A. and Patel,D.J. (1996) Structural basis of RNA folding and recognition in an AMP-RNA aptamer complex. *Nature*, **382**, 183–186.
21. Nonin,S., Leroy,J.L. and Gueron,M. (1995) Terminal base pairs of oligodeoxynucleotides: imino proton exchange and fraying. *Biochemistry*, **34**, 10652–10659.
22. Gueron,M., Kochoyan,M. and Leroy,J.L. (1987) A single mode of DNA base-pair opening drives imino proton exchange. *Nature*, **328**, 89–92.
23. Nonin,S., Jiang,F. and Patel,D.J. (1997) Imino proton exchange and base-pair kinetics in the AMP-RNA aptamer complex. *J. Mol. Biol.*, **268**, 359–374.
24. Nonin-Lecomte,S., Lin,C.H. and Patel,D.J. (2001) Additional hydrogen bonds and base-pair kinetics in the symmetrical AMP-DNA aptamer complex. *Biophys. J.*, **81**, 3422–3431.
25. Ferre-D'Amare,A.R., Zhou,K. and Doudna,J.A. (1998) Crystal structure of a hepatitis delta virus ribozyme. *Nature*, **395**, 567–574.
26. Williams,K.P. and Bartel,D.P. (1998) The tmRNA Website. *Nucleic Acids Res.*, **26**, 163–165.
27. Nameki,N., Chattopadhyay,P., Himeno,H., Muto,A. and Kawai,G. (1999) An NMR and mutational analysis of an RNA pseudoknot of *Escherichia coli* tmRNA involved in trans-translation. *Nucleic Acids Res.*, **27**, 3667–3675.
28. Kolk,M.H., van der Graaf,M., Wijmenga,S.S., Pleij,C.W., Heus,H.A. and Hilbers,C.W. (1998) NMR structure of a classical pseudoknot: interplay of single- and double-stranded RNA. *Science*, **280**, 434–438.
29. Michiels,P.J., Versleijen,A.A., Verlaan,P.W., Pleij,C.W., Hilbers,C.W. and Heus,H.A. (2001) Solution structure of the pseudoknot of SRV-1 RNA, involved in ribosomal frameshifting. *J. Mol. Biol.*, **310**, 1109–1123.
30. Chamorro,M., Parkin,N. and Varmus,H.E. (1992) An RNA pseudoknot and an optimal heptameric shift site are required for highly efficient ribosomal frameshifting on a retroviral messenger RNA. *Proc. Natl Acad. Sci. USA*, **89**, 713–717.
31. Ivanov,P.V., Zvereva,M.I., Shpanchenko,O.V., Dontsova,O.A., Bogdanov,A.A., Aglyamova,G.V., Lim,V.I., Teraoka,Y. and Nierhaus,K.H. (2002) How does tmRNA move through the ribosome? *FEBS Lett.*, **514**, 55–59.
32. Shpanchenko,O.V., Zvereva,M.I., Ivanov,P.V., Bugaeva,E.Y., Rozov,A.S., Bogdanov,A.A., Kalkum,M., Isaksson,L.A., Nierhaus,K.H. and Dontsova,O.A. (2005) Stepping transfer messenger RNA through the ribosome. *J. Biol. Chem.*, **280**, 18368–18374.
33. Wower,I.K., Zwieb,C. and Wower,J. (2005) Transfer-messenger RNA unfolds as it transits the ribosome. *RNA*, **11**, 668–673.
34. Yusupova,G.Z., Yusupov,M.M., Cate,J.H. and Noller,H.F. (2001) The path of messenger RNA through the ribosome. *Cell*, **106**, 233–241.